

Formation of Bi_2WO_6 nanocrystals under conditions of hydrothermal treatment

A. S. Svinolupova^{1,2}, M. S. Lomakin³, S. A. Kirillova², O. V. Almjashaeva³

¹St. Petersburg State Institute of Technology, Moskovsky Pr., 26, St. Petersburg, 190013, Russia

²St. Petersburg Electrotechnical University “LETI”, Professor Popov St. 5, St. Petersburg, 197376, Russia

³Ioffe Institute, Politekhnicheskaya St. 26, St. Petersburg, 194021, Russia

assvinolupova@etu.ru, almjasheva@mail.ru

PACS 81.07.Wx, 81.07.-b

DOI 10.17586/2220-8054-2020-11-3-338-344

Nanocrystalline Bi_2WO_6 was synthesized by means of hydrothermal treatment. It was shown that the formation rate of bismuth tungstate nanocrystals was determined by the presence of clusters formed at the stage of precipitation and having the same structure as that of Bi_2WO_6 , and the morphology of particles formed during hydrothermal treatment depended on the hydrothermal medium's pH.

Keywords: nanoparticles, nanocrystals, hydrothermal synthesis, bismuth tungstate.

Received: 3 June 2020

1. Introduction

Currently, materials based on perovskite-like oxides are of great interest, since they are characterized by a wide spectrum of functional properties, which make them promising products with respect to various technical fields [1–5]. Bismuth tungstate, a compound with a laminated perovskite-like structure of the Aurivillius phase type $(\text{Bi}_2\text{O}_2)^{2+}(\text{A}_{n-1}\text{B}_n\text{O}_{3n+1})^{2-}(\text{Bi}_2\text{WO}_6)$ that has a wide spectrum of important functional characteristics is one of the most in-demand materials [6–14].

To obtain Bi_2WO_6 , different methods may be applied, including the solid-phase synthesis [15], solution burning [16–18], microwave heating [19], sol-gel technique [20], solvothermal reaction [21, 22], electro spinning [23, 24], hydrothermal synthesis [25–30], etc. The most common methods include soft chemistry processes [7–9, 16–21, 25–30], among which a hydrothermal treatment method should be emphasized [7–9, 25–30]. The hydrothermal or solvothermal synthesis popularity is due to the possibility of obtaining bismuth tungstate in one step.

It should be noted that varying the synthesis procedures usually leads to variation in the structure, particle size, particle size distribution, morphology, which, in turn, significantly affects the synthesized compound's functional characteristics [6–30].

Thus, it is important to understand mechanisms of formation of the compounds depending on the synthesis conditions for the synthesis of materials with specified properties. Therefore, the objective of this study is to examine the effect of hydrothermal treatment conditions on the formation process and morphology of nanostructured Bi_2WO_6 .

2. Experimental

Aqueous solutions of bismuth (III) nitrate $(\text{Bi}(\text{NO}_3)_3 \cdot 5\text{H}_2\text{O})$, AR grade, GOST 4110-75) and sodium tungstate $(\text{Na}_2\text{WO}_4 \cdot 2\text{H}_2\text{O})$, AR grade, GOST 18289-78) were used as the starting materials for bismuth tungstate synthesis.

The separately prepared bismuth nitrate solution in nitric acid – acidified distilled water and sodium tungstate aqueous solution were mixed in the stoichiometric ratio and stirred using a mechanical agitator for 30 minutes (BWO_start). Then, a concentrated (12 M) aqueous solution of ammonium hydroxide (NH_4OH) , CP, GOST 3760-79) was added, to achieve a specified pH value. The pH values varied in the range from 2 to 13.

The hydrothermal treatment was performed in a steel autoclave with a teflon liner. The hydrothermal treatment temperature was 120, 150, 180 °C, the pressure was 70 MPa, and the isothermal time was 0.5 – 20 h. The obtained sediment was separated by decantation, flushed with distilled water and dried to a constant weight at 80 °C.

To study the effect of the starting components' pre-history on the formation process of bismuth tungstate under hydrothermal conditions, four variants of an initial suspension have been used as the starting material, and the suspension was obtained by mixing the aqueous solutions of sodium tungstate and bismuth nitrate, with the addition of ammonium hydroxide solution until pH = 10 (BWO_init):

- (1) the initial suspension was subjected to hydrothermal treatment without flushing or any additional procedures ($T = 180$ °C, $P = 70$ MPa, $\tau = 2$ h) – sample BWO_init.HT;

- (2) the initial suspension was filtered (without flushing) and dried at 80 °C (sample – BWO_init_dry), then the powder was subjected to hydrothermal treatment ($T = 180$ °C, $P = 70$ MPa, $\tau = 2$ h) – sample BWO_init_dry_HT;
- (3) the initial suspension was flushed with distilled water to remove impurity ions, until pH = 7 and the absence of NO_3^- and subjected to hydrothermal treatment ($T = 180$ °C, $P = 70$ MPa, $\tau = 2$ h) – sample BWO_clean_HT;
- (4) the initial suspension was flushed with distilled water to remove impurity ions, until pH = 7 and the absence of NO_3^- , dried at 80 °C (sample BWO_clean_dry) and subjected to hydrothermal treatment ($T = 180$ °C, $P = 70$ MPa, $\tau = 2$ h) – sample BWO_clean_dry_HT.

The elemental composition was determined by X-ray fluorescence analysis (XRF) (using Spectrascan Max GF2E) and by energy-dispersive X-ray spectroscopy (EDX) with the use of a scanning electron microscope (Vega3 Tescan and FEI Quanta-200) with EDAX energy-dispersive analyzer.

The samples' phase composition was analyzed by means of X-ray powder diffraction, using RigakuSmartLab 3 X-ray diffractometer ($\text{CoK}\alpha$ -radiation). The peaks in the diffractogram were identified using PDWin 4.0 software package and Crystallographica Search-Match package. The mean crystallite size was assessed by way of X-ray diffraction line profile analysis, using the Scherrer formula and a software package (SmartLabStudio III).

The obtained materials' morphology was studied by means of scanning electron microscopy (Tescan Vega3 microscope).

The IR-spectroscopy was carried out using Shimadzu IRTracer-100 spectrometer equipped with LabSolutions IR software.

3. Results and discussion

The ratio of elements in all of the non-flushed samples corresponded to the vicinity of bismuth tungstate singular point (Table 1), within the predetermined error tolerance.

TABLE 1. The results of elemental analysis of the studied materials

Sample	Molar ratio Bi/W	
	XRF	EDX
BWO_init_HT	2.2	1.9
BWO_init_dry	2.2	–
BWO_init_dry_HT	2.2	–
BWO_clean_HT	2.6	–
BWO_clean_dry	2.8	–
BWO_clean_dry_HT	2.8	–

As follows from Table 1, when the suspension is flushed, a change in the Bi/W ratio, i. e. an increase in bismuth content occurs. This may be due to the fact that at pH = 10 some portion of tungsten passes into solution as a result of the interaction with excessive NH_4OH and is removed from the system during decantation.

It should also be noted that, within the methods sensitivity, the samples following hydrothermal treatment contained no impurity elements (Na), the presence of which may be associated with the starting reagents' chemical composition.

The results of X-ray analysis of the samples following hydrothermal treatment are presented in Fig. 1(a,b). According to X-ray diffraction data, when a suspension with no additional treatment (Fig. 1(b), BWO_init_HT) is used as the starting material for hydrothermal synthesis, X-ray peaks corresponding only to Bi_2WO_6 are observed (ICSD code 73-1126). The size of Bi_2WO_6 crystallites is approximately 30 nm. If the suspension is first flushed with distilled water until neutral pH, then, following hydrothermal treatment, the X-ray diffractogram will show peaks indicating the predominant formation of bismuth oxide ($\delta\text{-Bi}_2\text{O}_3$), with an insignificant amount of Bi_2WO_6 (Fig. 1(b) BWO_clean_HT). In this case, the tungsten-containing component appears to be washed out of the immediate surrounding of $\text{Bi}(\text{OH})_3$, which contributes to $\delta\text{-Bi}_2\text{O}_3$ formation during hydrothermal treatment of the composition.

After the initial suspension drying at 80 °C, an X-ray amorphous powder was formed (Fig. 1(a), BWO_init_dry), the hydrothermal treatment of which at 180 °C for 2 hours did not lead to any noticeable changes in the phase state

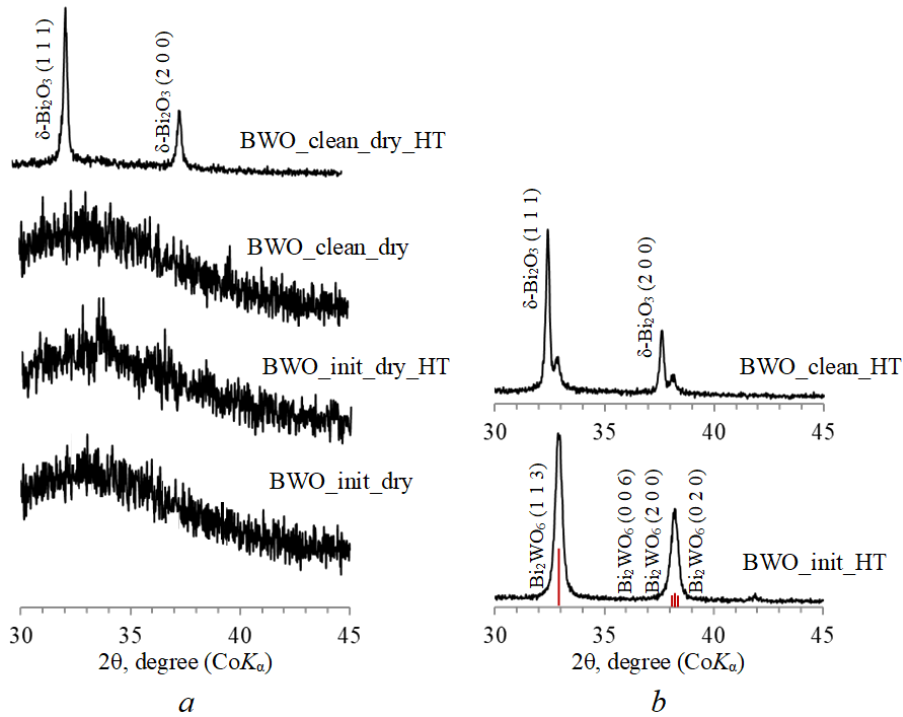


FIG. 1. X-ray diffractograms of the samples with various pre-histories of the initial suspension: a – the suspensions were dried; b – the suspensions were not dried

(Fig. 1(a), BWO_init_dry_HT). Drying of the flushed suspension (sample BWO_clean_dry) led to formation of X-ray amorphous powder (Fig. 1(a), BWO_clean_dry), as well as in the case with no flushing procedure. However, following hydrothermal treatment, a crystalline phase was formed, which was solely presented by δ - Bi_2O_3 (Fig. 1(a), BWO_clean_dry_HT). It should be noted that the size of δ - Bi_2O_3 crystallites was about 70 nm for all samples, which is significantly greater than that of Bi_2WO_6 crystallites formed as a result of hydrothermal treatment (Fig. 1(b), BWO_init_HT).

Note that for the synthesis of ZrO_2 [31], CoFe_2O_4 [32], BiFeO_3 [33, 34] nanoparticles, there was a substantial difference in the samples' phase state following hydrothermal treatment of precipitated hydroxides – without their preliminary drying and after drying. Such differences seem to be associated with a change in the initial amorphous deposit composition and structure as a result of its thermal processing.

Since the suspension flushing and drying appeared to result in a change in the hydrothermal medium pH value from 10 to 7, the effect of pH on the crystallization process was studied. A suspension obtained with no flushing and drying (BWO.start) was used as the starting material. The medium acidity was 2, 8, 10, 13. The hydrothermal treatment temperature was 180 °C, the pressure was 70 MPa, and the duration was 2 h.

The results of elemental analysis are presented in Table 2. The results of X-ray diffraction analysis and morphological analysis of the obtained materials are presented in Fig. 2.

TABLE 2. The results of the studied materials' elemental analysis, following hydrothermal treatment at 180 °C for 20 h

pH	Molar ratio Bi/W	
	XRF	EDX
2	2.1	2.0
8	2.2	1.9
13	2.1	1.9

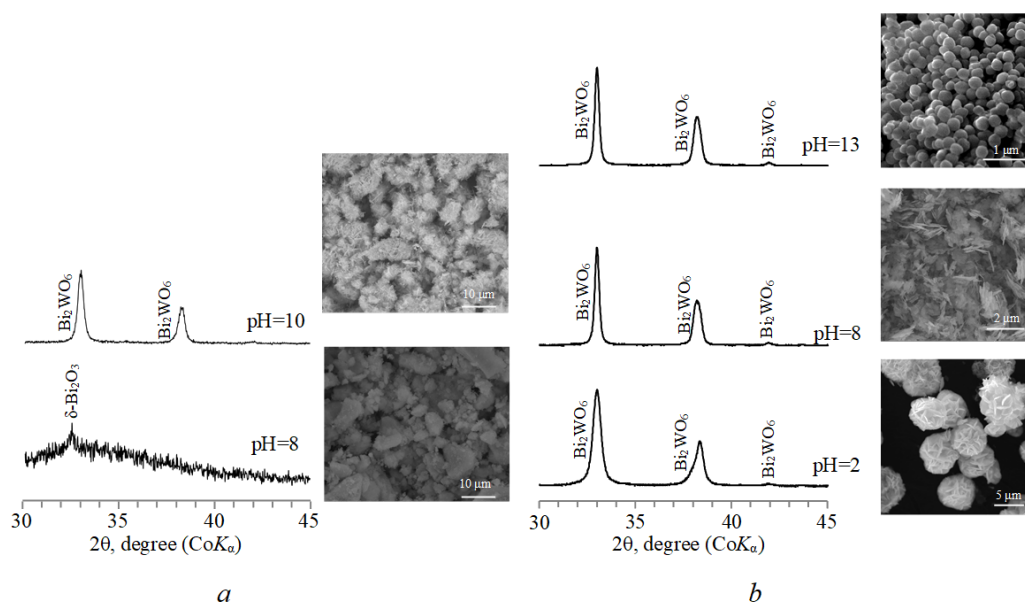


FIG. 2. X-ray diffractograms and microphotographs of the samples at various pH values of the hydrothermal medium. Hydrothermal treatment conditions: temperature of 180 °C, pressure of 70 MPa, isothermal time of 2 h (a) and 20 h (b)

Hydrothermal treatment of the sample BWO_start at the medium pH = 8 and the isothermal time of 2 h did not lead to bulk crystallization: only insignificant intensity reflection corresponding to crystalline $\delta\text{-Bi}_2\text{O}_3$ was observed in the X-ray diffractogram (Fig. 2(a)). Additionally, the sample was mostly presented by large, rather dense agglomerates (Fig. 2(a)), which is characteristic of materials in the X-ray amorphous state. An increase in the hydrothermal medium pH resulted in active crystallization process (Fig. 2(a)); peaks corresponding to crystalline Bi_2WO_6 with a crystallite size of about 25 nm were observed in the X-ray diffractogram. According to scanning electron microscopy data, the sample is represented by the agglomerates of particles of non-isometric shape, with a thickness of significantly less than 1 μm and a length of several μm .

When the hydrothermal treatment duration is increased to 20 h, crystalline bismuth tungstate formation is observed (Fig. 2(b)), irrespective of the medium pH value; and an increase in the pH values results in the narrowing of X-ray diffraction lines, which reflects an increase in the formed crystallites' size: from 23 nm at pH = 2 to 50 nm at pH = 13. It should be noted that the change in pH is accompanied by a significant change in the formed particles' morphology (Fig. 2(b)). In acidic conditions (pH = 2), flower-like agglomerates consisting of plates, with a size of 5 – 7 μm and a thickness of several hundred nanometers are formed. The sample obtained in mildly alkaline conditions is represented by unstructured plates with a thickness of 100 – 500 nm. The hydrothermal treatment of BWO_init in strongly alkaline conditions (pH = 13) results in the formation of spherical particles with a diameter from 200 to 700 nm (Fig. 2(b)).

Thus, basing on the presented data, it can be concluded that bismuth oxide ($\delta\text{-Bi}_2\text{O}_3$) is first crystallized, and then bismuth tungstate is formed during the hydrothermal treatment. In alkaline conditions, the formation rate of Bi_2WO_6 is significantly higher due to tungsten passing into solution, which contributes to the mass transfer process. The effect of pH may also be responsible for processes observed when varying the initial suspension pre-history. If a suspension subjected to no additional treatment is used, then the hydrothermal medium pH is equal to 10, and the formation rate of Bi_2WO_6 is so high that no intermediate product ($\delta\text{-Bi}_2\text{O}_3$) can be observed (Fig. 1, BWO_init). All other samples are subjected to a drying procedure, and the stock solution is decanted, which appears to result in lower pH values and thus a lower formation rate of both the intermediate product, and the end product, i.e. bismuth tungstate. The initial suspension flushing not only leads to a lower pH value, it may also lead to tungsten “washing out” of the system and to a deviation from the components' stoichiometric ratio (Table 1), which results in a lower formation rate of Bi_2WO_6 . Moreover, spatial separation of the system components is likely to occur during the suspension flushing and subsequent drying, which hinders the formation of Bi_2WO_6 under these conditions.

As a result of comparing the IR-spectra of pure bismuth- and tungsten-containing components of the system $\text{Bi}_2\text{O}_3\text{-WO}_3\text{-H}_2\text{O}$ (Fig. 3, curves 1 and 2) and the spectrum of the initial composition obtained by co-precipitation, i.e. of the sample BWO_init_dry (Fig. 3, curve 3), it can be concluded that clusters with a short-range order similar to the end product structure are formed during precipitation in the system. This is evidenced by, e. g., spectral

lines $\sim 780\text{ cm}^{-1}$ observed in the IR-spectra of the co-precipitated mixture but not present in the spectra of individual components of the system, and spectral lines $\sim 730\text{ cm}^{-1}$ corresponding to W–O bonds within Bi_2WO_6 [35–37]. It seems to be the number of such clusters in the co-precipitated sample that determines the activity of formation of either Bi_2WO_6 , or $\delta\text{-Bi}_2\text{O}_3$.

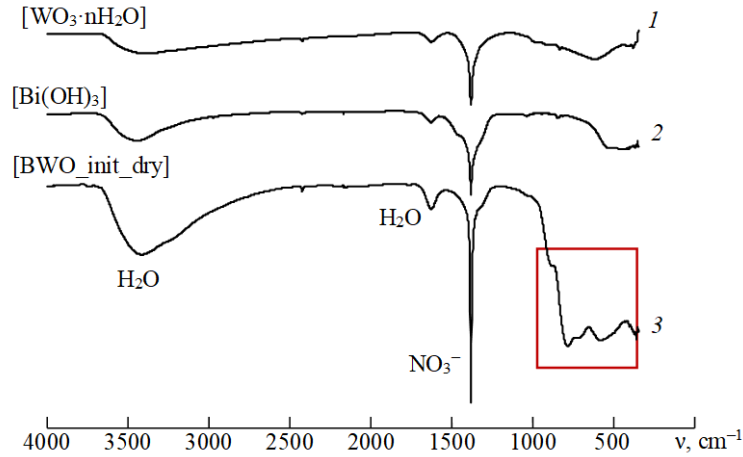


FIG. 3. IR-spectra of the samples obtained by precipitation

An initial suspension (BWO_init) was used as the starting material, and the hydrothermal medium pH 10 was maintained for studying the formation rate of Bi_2WO_6 at various temperatures of hydrothermal treatment. The elemental composition of the obtained samples is presented in Table 3.

TABLE 3. The results of elemental analysis of the test materials

$T, ^\circ\text{C}$	τ, hours	Molar ratio Bi/W	
		XRF	EDX
120	1	2.19	–
	2	2.18	–
	4	2.21	–
150	1	–	2.23
	2	–	2.05
	4	–	2.11
180	0.5	–	1.85
	1	–	2.23
	1.5	–	1.97
	2	–	2.04

As indicated by the data presented in Fig. 4, the formation rate of bismuth tungstate to a significant degree depends on the hydrothermal treatment temperature. At the hydrothermal treatment temperature of $120\text{ }^\circ\text{C}$, almost trace quantity of bismuth tungstate is observed after 4 hours (Fig. 4(a)). If the temperature is increased to $150\text{ }^\circ\text{C}$, Bi_2WO_4 will be completely formed within the same period, and an additional increase by $30\text{ }^\circ\text{C}$ will result in the completion of bismuth tungstate crystallization in 2 hours (Fig. 4(a)). The formed bismuth tungstate crystallite size is about 30 nm, and it does not change as the hydrothermal treatment duration is increased (Fig. 4(b)).

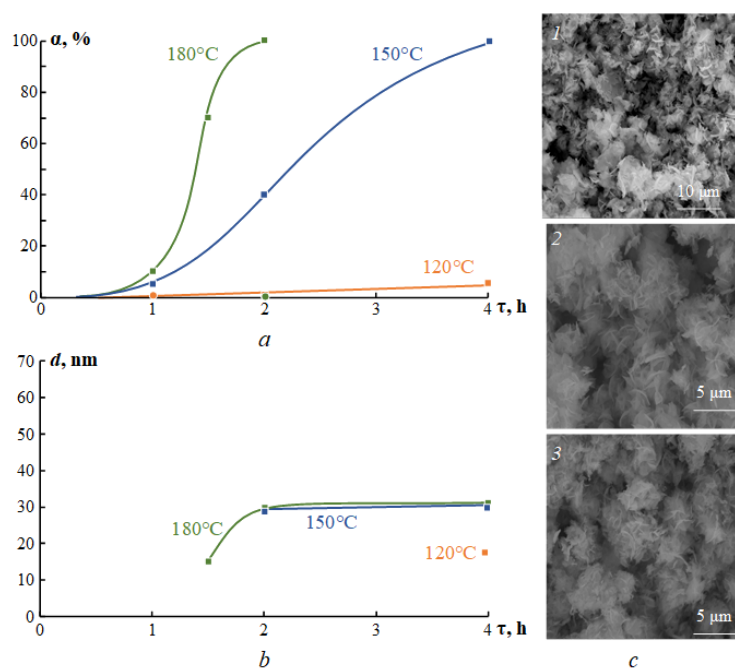


FIG. 4. Crystallization degree (a), crystallite size (b) and morphology (c) as a function of hydrothermal treatment temperature and duration: 1c – $T = 150\text{ }^{\circ}\text{C}$, $\tau = 4\text{ h}$; 2c – $T = 180\text{ }^{\circ}\text{C}$, $\tau = 1.5\text{ h}$; 3c – $T = 180\text{ }^{\circ}\text{C}$, $\tau = 2\text{ h}$

As it follows from scanning electron microscopy data (Fig. 4(c)), changes in the hydrothermal treatment temperature and duration produce almost no effect on the formed particles' morphology. In all cases, particles of a non-isometric (plate-like) shape with a thickness of 100 – 500 nm and a plate width of up to 5 μm are formed. According to the results of X-ray diffraction line broadening analysis, the plates observed in Fig. 4(c) consist of crystallites with a size of about 30 nm. And both the particle size (Fig. 4(c)) and the crystallite size (Fig. 4(b)) remain almost unaffected by an increase in the hydrothermal treatment temperature and duration.

4. Conclusion

Thus, the presented data allows us to conclude that clusters with a Bi_2WO_6 -like structure are formed at the stage of precipitation, and the presence of such clusters to a significant degree determines the formation rate of bismuth tungstate nanocrystals. It should also be noted that the morphology of the particles formed during hydrothermal treatment depends on the hydrothermal medium's pH.

Acknowledgements

The authors express their gratitude to V. V. Gusarov for the attention he paid to the work.

X-ray diffraction and SEM was performed using the equipment of the Engineering Center Saint Petersburg State Institute of Technology.

This study was financially supported by the Russian Science Foundation (project no. 16-13-10252).

References

- [1] Pattanayak S., Choudhary R.N.P. Synthesis, electrical and magnetic characteristics of Nd-modified BiFeO_3 . *Ceramics International*, 2015, **41** (8), P. 9403–9410.
- [2] Popkov V.I., Almjasheva O.V., et al. Magnetic properties of YFeO_3 nanocrystals obtained by different soft-chemical methods. *Journal of Materials Science: Materials in Electronics*, 2017, **28** (10), P. 7163–7170.
- [3] Kaur P., Singh K. Review of perovskite-structure-related cathode materials for solid oxide fuel cells. *Ceramics International*, 2020, **46** (51), P. 5521–5535.
- [4] Martinson K.D., Ivanov V.A., et al. Facile combustion synthesis of TbFeO_3 nanocrystals with hexagonal and orthorhombic structure. *Nanosyst.: Phys. Chem. Math.*, 2019, **10** (6), P. 694–700.
- [5] Lomanova N.A., Tomkovich M.V., et al. Magnetic Properties of $\text{Bi}_{1-x}\text{Ca}_x\text{FeO}_{3-\delta}$ Nanocrystals. *Physics of the Solid State*, 2019, **61**, P. 2535–2541.

- [6] Lin X., Liu Z., et al. Controllable synthesis and photocatalytic activity of spherical, flower-like and nanofibrous bismuth tungstates. *Mater. Sci. Eng. B*, 2014, **188**, P. 35–42.
- [7] Liu Y., Ding Z., et al. Hydrothermal synthesis of hierarchical flower-like Bi_2WO_6 microspheres with enhanced visible-light photoactivity. *Mater. Lett.*, 2015, **157**, P. 158–162.
- [8] Phuruangrat A., Maneechote A., et al. Effect of pH on visible-light-driven Bi_2WO_6 nanostructured catalyst synthesized by hydrothermal method. *Superlattice. Microst.*, 2015, **78**, P. 106–115.
- [9] Ge M., Liu L. Sunlight-induced photocatalytic performance of Bi_2WO_6 hierarchical microspheres synthesized via a relatively green hydrothermal route. *Mater. Sci. Semicond. Process.*, 2014, **25**, P. 258–263.
- [10] Er X., Zhang Y., et al. Atomic structure of domain and defect in layered-perovskite Bi_2WO_6 thin films. *Mater. Charact.*, 2019, **154**, P. 395–399.
- [11] Utkin V.I., Roginskaya Y.E., et al. Dielectric properties, electrical conductivity, and relaxation phenomena in ferroelectric Bi_2WO_6 . *Phys. Status Solidi A – Appl. Mater. Sci.*, 1980, **59** (1), P. 75–82.
- [12] Kudo A., Hijii S. H_2 or O_2 evolution from aqueous solutions on layered oxide photocatalysts consisting of Bi^{3+} with $6s^2$ configuration and dtransition metal ions. *Chem. Lett.*, 1990, **28** (10), P. 1103–1104.
- [13] Zhang Q., Jiang Z., Wang M., Ge X. Gamma ray radiation effect on Bi_2WO_6 photocatalyst. *Chin. J. Chem. Phys.*, 2018, **31** (5) P. 701–706.
- [14] Wang D., Zhen Y., et al. Synthesis of mesoporous Bi_2WO_6 architectures and their gas sensitivity to ethanol. *J. Mater. Chem. C1*, 2013, **26**, P. 4153–4162.
- [15] Finlayson A.P., Ward E., Tsaneva V.N., Glowacki B.A. Bi_2O_3 – WO_3 compounds for photocatalytic applications by solid state and viscous processing. *Journal of Power Sources*, 2005, **145** (2), P. 667–674.
- [16] Zhang Z.J., Wang W.Z., et al. Low-temperature combustion synthesis of Bi_2WO_6 nanoparticles as a visible-light-driven photocatalyst. *J. Hazard. Mater.*, 2010, **177**, P. 1013–1018.
- [17] Zawawi S.M.M., Yahya R., et al. Structural and optical characterization of metal tungstates (MWO_4 ; M = Ni, Ba, Bi) synthesized by a sucrose-templated method. *Chem. Cent. J.*, 2013, **7** (1), P. 80–90.
- [18] Yu S.-H., Liu B., et al. General synthesis of single-crystal tungstate nanorods/nanowires: a facile low-temperature solution approach. *Advanced Functional Materials*, 2003, **13**, P. 639–647.
- [19] Phu N.D., Hoang L.H., et al. Study of photocatalytic activities of Bi_2WO_6 nanoparticles synthesized by fast microwaveassisted method. *J. Alloys. Compd.*, 2015, **647**, P. 123–128.
- [20] Zhang G.K., Lu F., et al. Synthesis of nanometer Bi_2WO_6 synthesized by sol-gel method and its visible-light photocatalytic activity for degradation of 4BS. *J. Phys. Chem. Solids*, 2010, **71**, P. 579–582.
- [21] Zhu J., Wang J.G., et al. Solvothermal synthesis of highly active Bi_2WO_6 visible photocatalyst. *Res. Chem. Intermed.*, 2009, **35**, P. 799–806.
- [22] Xu C.X., Wei X., et al. Solvothermal preparation of Bi_2WO_6 nanocrystals with improved visible light photocatalytic activity. *Mater. Lett.*, 2009, **63**, P. 2194–2197.
- [23] Shang M., Wang W., et al. A practical visible-light-driven Bi_2WO_6 nanofibrous mat prepared by electrospinning. *J. Mater. Chem.*, 2009, **19** (34), P. 6213–6218.
- [24] Zhao G., Liu S.W., et al. Fabrication of electrospun Bi_2WO_6 microbelts with enhanced visible photocatalytic degradation activity. *J. Alloys Compd.*, 2013, **578**, P. 12–16.
- [25] Xu F., Xu C., et al. The synthesis of $\text{Bi}_2\text{S}_3/2\text{D}$ – Bi_2WO_6 composite materials with enhanced photocatalytic activities. *J. Alloys Compd.*, 2019, **780**, P. 634–642.
- [26] Liu Y., Tang H., et al. Self-assembled three-dimensional hierarchical Bi_2WO_6 microspheres by sole-gele-hydrothermal route. *Ceram. Int.*, 2014, **40**, P. 6203–6209.
- [27] Amano F., Nogami K., Abe R., Ohtani B. Preparation and characterization of bismuth tungstate polycrystalline flake-ball particles for photocatalytic reactions. *J. Phys. Chem. C*, 2008, **112**, P. 391–401.
- [28] Lomakin M.S., Proskurina O.V., Gusarov V.V. Influence of hydrothermal synthesis conditions on the composition of the pyrochlore phase in the Bi_2O_3 – Fe_2O_3 – WO_3 system. *Nanosyst.: Phys. Chem. Math.*, 2020, **11** (2), P. 246–251.
- [29] Zhang Z., Lin Y., Liu F. Preparation, crystallization and properties of Bi_2WO_6 nanoparticles. *Colloids and Surfaces A*, 2020, **5905**, 124493.
- [30] Tahmasebi N., Maleki Z., Farahnak P. Enhanced photocatalytic activities of $\text{Bi}_2\text{WO}_6/\text{BiOCl}$ composite synthesized by one-step hydrothermal method with the assistance of HCl. *Mater. Sci. Semicond. Process.*, 2019, **89**, P. 32–40.
- [31] Sharikov F.Yu., Almjasheva O.V., Gusarov V.V. Thermal analysis of formation of ZrO_2 nanoparticles under hydrothermal conditions. *Russ. J. Inorg. Chem.*, 2006, **51** (10), P. 1538–1542.
- [32] Kuznetsova V.A., Almjasheva O.V., Gusarov V.V. Influence of microwave and ultrasonic treatment on the formation of CoFe_2O_4 under hydrothermal conditions. *Glass Physics and Chemistry*, 2009, **35** (2), P. 205–209.
- [33] Proskurina O.V., Abiev R.S., et al. Formation of nanocrystalline BiFeO_3 during heat treatment of hydroxides co-precipitated in an impinging-jets microreactor. *Chemical Engineering and Processing – Process Intensification*, 2019, **143**, 107598.
- [34] Proskurina O.V., Nogovitsin I.V., et al. Formation of BiFeO_3 Nanoparticles Using Impinging Jets Microreactor. *Russ. J. Gen. Chem.*, 2018, **88** (10), P. 2139–2143.
- [35] Xia J.X., Di J., et al. Facile fabrication of the visible-light-driven $\text{Bi}_2\text{WO}_6/\text{BiOBr}$ composite with enhanced photocatalytic activity. *RSC Advances*, 2014, **4**, P. 82–90.
- [36] Qamar M., Elsayed R.B., et al. Highly efficient and selective oxidation of aromatic alcohols photocatalyzed by nanoporous hierarchical $\text{Pt}/\text{Bi}_2\text{WO}_6$ in organic solvent-free environment. *ACS Applied Materials & Interfaces*, 2015, **7** (2), P. 1257–1269.
- [37] Liu L., Qi Y., et al. Dramatic activity of a $\text{Bi}_2\text{WO}_6@g\text{-C}_3\text{N}_4$ photocatalyst with a core@shell structure. *RSC Advances*, 2015, **5** (120), P. 99339–99346.